'TORUS': A slotless, toroidal-stator, permanent-magnet generator

E. Spooner, MIEE
B.J. Chalmers, FIEE

Abstract: TORUS is a compact electrical machine particularly suitable for use as an engine-driven generator and which, when supplied via suitable switching circuits, can operate as a brushless DC motor to start the engine. The machine is of simple and cheap construction and gives high efficiency. The use of Neodymium-Iron-Boron permanent magnets gives good utilisation and small overall size and weight. Several 2.5 kW prototype machines have been built and tested, and have demonstrated all aspects of performance and capability of the TORUS configuration in the generating mode.

List of symbols

A = Area of ventilating air passage, m^2
B_g = Airgap mean flux density over the poles, T
B_p = Peak flux density of a sinusoidal distribution, T
E = Phase maximum EMF, V
F = Ventilating air flow, m^3/sec
I = Current, A
J_1 = Effective mean electric loading, A/m, at the stator inner radius
L = Inductance, H
P = Fan pressure, N/m^2
P_E = Eddy current loss, W
P_J = I^2R loss, W
R_1, R_2 = Inner and outer radii of toroid, m
Q = Energy, J
T = Torque, Nm; Time duration of trapezoidal EMF plateau, sec
V = Output DC voltage, V (measured to winding star point)
c = Rotor/stator running clearance, m
d = Stator winding wire diameter, m
f = Frequency, Hz
k = Ratio of stator inner to outer radii
r = Phase resistance, Ω
t_m = Magnet thickness, m
t_w = Winding thickness, m
γ = Slope of sides of trapezoidal EMF wave, V/sec
μ_r = Magnet recoil permeability
ρ = Stator conductor resistivity, Ωm

τ = Time constant of phase winding, sec
ω = Electrical angular frequency, rad/sec

1 Introduction

TORUS is a compact lightweight electrical machine developed initially for use in a portable generator providing low voltage DC output. For portable generating equipment lightness and compactness are of great importance. High efficiency is also vital because it influences the quantity of fuel which must be carried. For a machine to deliver high power from a small space, it must have:

(a) High electric and magnetic loadings.

(b) Intensive cooling to remove the loss from the small volume.

(c) Low impedance to avoid pull-out.

TORUS makes use of sintered Neodymium-Iron-Boron for the magnets so that a high magnetic loading is achieved. Its disc rotors act naturally as fans and so good cooling of the stator winding is ensured even with a high electric loading. A slotless winding is used thus providing low values of phase self and mutual inductances because the magnetic gap is necessarily large and slot leakage is of course absent. Also, with the high magnetic loading, it is possible to generate the required EMF using a small number of winding turns and so resistances and inductances are low.

Thus, TORUS is inherently light and compact. In addition, its mechanical configuration makes it well suited for integration with the engine to form a compact unit. The machine is very short and so can be mounted directly on the engine output shaft, eliminating the need for separate bearings or couplings and its moment of inertia is such that the flywheel is redundant. In addition, it may operate as a brushless DC motor for starting the engine, eliminating the usual starter motor and gears.

The basic layout is shown in Fig. 1. A simple toroidal strip-wound stator core carries a slotless toroidal winding. The rotor comprises two discs carrying axially polarised magnets. Typical flux paths are shown in Fig. 2. The machine has similarities with several other configurations proposed in recent years including the axial-flux,

permanent-magnet machine investigated by Campbell [1] and the slotless, toroidal-stator alternator proposed by Evans and Eastham [2]. Some aspects of the design of the present machine have been described earlier [3, 4].
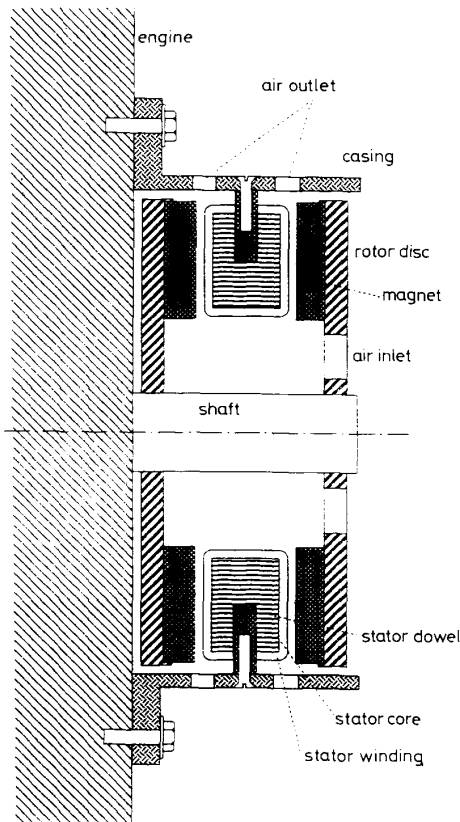

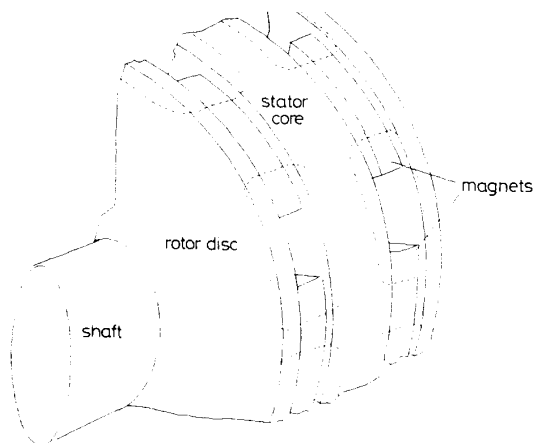**Fig. 1**   *Machine cross-section*

Fig. 2   *Principal flux paths (shown as dotted lines)*

The arrangement has not previously found widespread commercial application, partly because suitable magnets of high remanence and coercivity have not been available. It is interesting to note that in his studies of alternative machine topologies, [5], Laithwaite commented on the merits of a toroidal arrangement and indicated that this can yield significantly increased 'goodness factor'.

TORUS employs the comparatively new magnetic material Neodymium-Iron-Boron which has the neces-

sary remanence together with a coercivity which permits a slotless winding to be used, thus bringing further improvements over earlier designs.

Table 1 : Prototype machine dimensions (mm)

| Machine	1	2	3
Stator core OD	167	167	152
Stator core ID	96	96	92
Core axial thickness	35	35	30
Winding layers	1	1	2
Winding coils	22	18	18
Phases	11	9 (3)	9 (3)
Turn/coil	10	12	14
Wire diameter	1.06	1.06	1.5
Design J, kA/m	11.8	11.8	17.5
Self inductance μH/ph	120	175	130
Phase resistance at 120°C, mΩ	90	107	54
Magnet thickness	5	5	6
Airgap flux density (T)	0.61	0.61	0.55
Design EMF (DC) at 3000 RPM	36	42	36
Length of machine	70	70	68
Machine Mass (approx kg)	7.7	7.7	6.4
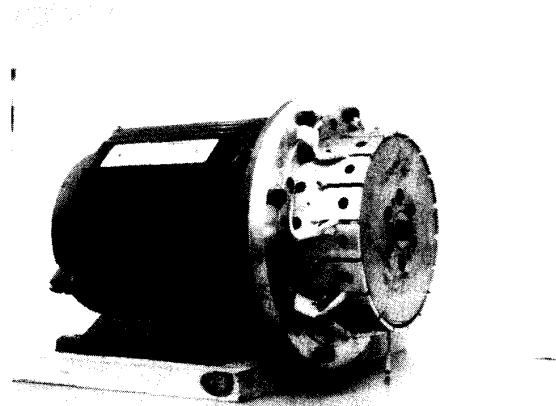
Fig. 3   *Prototype Machine 3 mounted on its drive motor*

Portable generating equipment is often required to provide a low voltage DC supply. The AC output of the machine is fed through rectifiers which are conveniently mounted on the stator casing which acts as a well-ventilated heat sink. It is usually important to avoid excessive ripple in the output voltage. The machine has therefore been designed to provide a flat-topped EMF wave. In addition, a large number of phases may be used to raise the frequency of the output ripple so that filtering can be performed with a few small passive components. Additional electronic components are required for brushless DC motor operation; these may also be fixed to the casing.

2   Experimental machines

Experimental machines have been built to two basic designs with an intended output of 2.5 kW at a constant speed of 3000 rpm. Machine 1 was based on a single-layer, 11-phase winding with 10 turns in each of the 22 coils. This machine was intended to deliver an output current of 89 A at 28 V DC. A 9-phase version was also built using 18 12-turn coils, the nominal output in this case is 73 A at 34 V. This is referred to as Machine 2. Since the rotors have six poles, successive phases of Machine 2 are separated electrically by 120° and may be connected with phases 1, 4 and 7 in parallel, phases 2, 5

Table 2: Calculated losses (W) for the experimental machines

Machine	1	2	3
Eddy	35	35	62
Iron	22	22	16
Windage	10	10	10
Total no-load loss	67	67	88
I^2R	493	508	245
Diode	178	146	178
Total loss	738	721	511
Efficiency, % (inc diodes)	77.4	77.6	83.0
Efficiency, % (exc diodes)	81.7	81.3	88.2

and 8 in parallel, and phases 3, 6 and 9 in parallel to form a simple three-phase output.

Machine 3 is constructed to a different basic design. Like Machine 2, it has a 9-phase winding, but each coil is constructed in two layers which leads to smaller overall machine dimensions. This construction was adopted to take advantage of the excellent cooling properties revealed by tests on the earlier machines. Design data for the three machines is presented in Table 1.

For testing purposes, each machine was built to be mounted directly on the flange of a 4 kW, 3000 RPM foot-flange TEFC induction motor. Fig. 3 shows Machine 3 mounted on its drive motor. The comparison in size between the 4 kW standard induction motor and the 2.5 kW experimental generator, which was not fitted with a separate fan, is quite striking.

Of the three machines, only Machine 3 successfully met its specification in all respects. This machine achieves the required output of 2.5 kW at 28 V DC with a temperature rise of the windings well inside normally accepted limits.

3 Loss mechanisms

Being excited by permanent magnets, the rotor suffers no significant loss. On the other hand, the machine incorporates integral output rectifiers and their loss may make a significant contribution to the total, especially since the machine is intended for low-voltage, high-current operation.

3.1 I^2R, (Joule loss)
This is the principal loss in the machine under most operating conditions although eddy-current loss is also significant and may be dominant at high speed. The toroidal configuration leads to somewhat lower I^2R loss than would otherwise occur because the end windings, that is the axial sections of each turn passing through the middle and over the outside of the core, are short. It is, of course, the RMS current which determines the loss and this can be rather higher than that expected from a straightforward consideration of the DC output current. Also, for applications requiring low voltage and high current, there are few turns in each stator coil and the connections between coils and to the rectifiers cannot be ignored.

3.2 Eddy current loss
The winding is located in the airgap and hence is situated in the main field. Motion of the magnets past the winding causes the field through each conductor to vary periodically and to induce eddy currents. Sinusoidal variation of a uniform field through round wires gives rise to a loss

in the conductor of

$$P_E = B_p^2 \omega^2 d^2 / 32\rho \quad \text{per unit conductor volume} \quad (1)$$

For rectangular-section conductors, the factor 32 is replaced by 24. Thus round wires are somewhat less prone to eddy-current loss. This compensates to some extent for the worse fill factor of round wire compared with rectangular conductors. Round wire, being easier to handle, has been chosen for all the prototype machines.

In cases where the phase current is large, thick wire is needed which leads to very high eddy current loss. The eddy current loss may be reduced by using conductor which is subdivided into a number of fine strands which are insulated from each other and transposed (i.e. twisted) to avoid circulating currents. This inevitably leads to a reduced copper section and to increased I^2R loss. The preferred option in all cases studied so far has been to use a large number of phases to reduce the required phase current.

The waveform of the flux density variation is deliberately made non-sinusoidal in this machine and even quite low-amplitude harmonics can lead to serious additional eddy-current loss; a sharp-edged rectangular wave would, in principle, lead to infinite loss. The real situation is not that bad because fringing of flux at the edges of the poles effectively eliminates the higher harmonics. In the design and performance calculations, the loss found from eqn. 1 is multiplied by an empirical factor determined by the mean pole pitch and the effective gap length and based on earlier work concerning eddy-current loss in slotless DC machines [6].

3.3 Iron loss
The core is strip-wound from 0.3 mm thick electrical steel and no punching takes place. The core works at fairly high flux density in the tangential direction but rather low flux density axially. The quantity of steel used is quite small. Taken together, these features lead to low iron loss. Although it has not been used for the prototypes, grain-oriented material would be ideal for this machine, allowing a somewhat higher tangential field to be used leading to a reduction of core weight and loss and a small reduction in the length of turn required, and consequent further small reductions in weight and loss. Amorphous iron alloys were considered, but rejected. Their poor space factor would call for increased axial length and hence increased weight and slightly increased copper loss.

3.4 Diode loss
TO-220 plastic-package rectifiers have been chosen because they can be mounted readily on the outer casing. Simple silicon diodes were the only form available in this package for the prototype machines. The diodes form a polyphase bridge and the output voltage is reduced by twice the forward voltage of a single diode. The total diode loss is equal to the DC output current multiplied by twice the forward voltage. Ideally, Schottky diodes with low forward voltage would be used but they were not available in the required package with suitable rating. The forward voltage is assumed constant for loss calculation, the value used (1.0 V) being measured for a typical diode carrying a current similar in value to the mean current during the conduction period at full-load operation.

3.5 Windage and fan loss
The usual design formulas for calculating windage loss in small machines (see Reference 11 for example) yield

values of around 0.2 W for the experimental machines. In addition, power is required to drive cooling air through the machines; the pressure and flow values presented in Section 6.1 correspond to a power of about 2 W for a fan of 100% efficiency. The magnets glued to the discs certainly do not operate at 100% efficiency as fan blades, so a nominal figure of 10 W is adopted to give some account of these losses in the loss summation. If high speed versions of the Torus machine are contemplated, however, it would be wise to consider these losses more carefully since they vary according to the square of the speed.

3.6 Loss summation

For the three prototype machines, calculated losses and efficiencies at the nominal rated load are given in Table 2. The I^2R losses are based on the RMS-to-mean current ratio determined by observation of phase current waveforms, (see Fig. 4). The eddy current and iron losses are
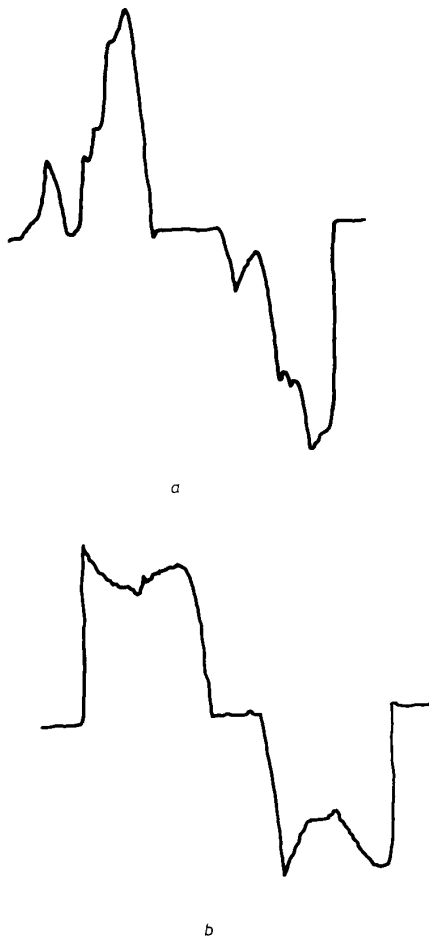

a

b

Fig. 4   *Measured phase currents*
a Machine 1
b Machine 2

predicted values and the rectifier loss is simply the product of the DC current and a constant diode forward voltage of 2 V.

The efficiency of Machine 3 in particular is unusually high for a machine of this rating. The improvement in efficiency achieved in the design of Machine 3 is due mostly to the large reduction in I^2R loss through the use

500

of thicker wire, though at the expense of increased eddy-current loss.

4   Electromagnetic design

4.1   Optimum proportions

4.1.1 Stator diameters: The torque is calculated as shown in the Appendix to this paper and is given by

$$T = B_g J_1 2\pi (R_2^2 - R_1^2) R_1 \qquad (2)$$

The distribution of current around the stator is complex in practice. It is assumed for eqn. 2 that all the current passes through wires which are in the full field of the magnets. The value of torque given by eqn. 2 is therefore a maximum figure.

The term: $(R_2^2 - R_1^2)R_1$ can be written $R_2^3 k(1 - k^2)$. For a given outside diameter and loadings, the torque may be maximised if k is chosen to maximise $k(1 - k^2)$. This is achieved with $k = 1/\sqrt{(3)}$.

4.1.2 Winding thickness: Copper losses are removed by heat transfer to the air flowing between rotor and stator and by conduction into the iron core. The rate at which heat may be removed is largely independent of the winding thickness, t_w, but the heat generated depends on the thickness and on the electric and magnetic loadings. The copper loss, P_C, has two components, I^2R or Joule loss, P_j, due to the passage of load current and eddy current loss, P_E, due to the main airgap flux passing through the wires.

$$P_j = C_j J_1^2 / t_w \qquad (3)$$

$$P_E = C_E B_g^2 t_w \qquad (4)$$

where C_J and C_E are constants for a particular set of values of pole number, speed, wire diameter, winding space factor and temperature.

An optimum winding thickness, t_{opt} exists which maximises the product $B_g J_1$ and hence the power capacity for a given value of P_C.

$$t_{opt} = \frac{P_C}{2 C_E B_g^2} \qquad (5)$$

If eqn. 5 is satisfied then the eddy current and I^2R losses are equal. However, in many cases, such as vehicle applications, the engine speed varies over a wide range. Since permanent magnets allow no control of excitation, B_g is fixed and C_E varies as (speed)^2 and so the eddy current loss may be excessive at high speeds. In an extreme case the eddy current loss alone could cause overheating even with the machine unloaded. Consequently, for such applications, the winding thickness would be chosen to be rather smaller than the value indicated in eqn. 5.

4.1.3 Design procedure: Many other aspects of the design are of importance and an optimum design cannot be readily defined or derived in simple closed form. Also several parameters such as the number of turns per coil and the available set of wire sizes are not continuous variables. A computer program has been employed, therefore, to evaluate a wide range of design variables for each specification considered. For the evaluation of diameters it is necessary to take account of output voltage regulation with load due to winding resistance and inductance and an iterative process is necessary. The temperatures are evaluated using the thermal model described in Section 6.2 and are used to adjust resistance values as the iteration of dimensions proceeds.

4.2 Magnet arrangement

4.2.1 Magnet shape: To reduce generated voltage ripple and because of the requirement to operate sometimes as a brushless DC motor, the magnets have been shaped to generate a flat-topped wave of EMF in each phase. Arc-shaped magnets would ideally be used but it would be difficult and wasteful to cut arcs from readily available rectangular slabs. Instead trapezoidal poles built from three pieces were used in the first design, Machines 1 and 2 (see Fig. 5).

The magnets used are of Neodymium-Iron-Boron. The remanence, B_r, of the grade used in the first design is approximately 1.15 T and the coercivity is approximately 800 kA/m. The flux density generated by the magnets is found by considering the reluctances of the magnets and of the airgap through which the flux must pass. If fringing is ignored then the flux density at the stator is given by

$$B_g = B_r t_m / \{t_m + \mu_r(t_w + c)\} \qquad (6)$$

If the magnets were annular arcs with the same radii as the core, then leakage at the edges would cause the average flux density to be a little less than indicated by eqn. 6. However, in some regions, the magnets extend radially beyond the stator core at either the inner or outer edge, as shown in Figs. 5a and b, and so the effective areas of the magnets and the gap are a little greater than the corresponding area of the stator core. Consequently, leakage at the edges of the magnet is compensated by a contribution to the useful flux from the fringe.

In Machine 1, the expected mean flux density is 0.61 T which would generate an EMF of 17.6 V at a speed of 3000 RPM. The observed EMF has just this magnitude. The waveform is shown in Fig. 5c. It is apparent that variations in the contribution from the fringe field cause the undesirable ripple on the top of the otherwise trapezoidal wave. The maximum EMF is induced when the coil is aligned with the radius marked X in Fig. 5a.

Because, of the difficulty of assembling the three-piece magnets, Machine 3 used the two-piece arrangement shown in Fig. 6a. This is a closer approximation to the ideal arc shape and the magnet is, in this case, made to overhang the core considerably at both the inside and outside edges to take full advantage of the fringe field. The material used in this machine has $B_r = 1.08$ T and the flux density given by eqn. 6 is 0.55 T which would lead to an induced EMF of 17.7 V at 3000 rpm. The EMF actually measured is shown in Fig. 6b, and has a maximum value of 19.2 V, indicating a valuable addition of 8% to the flux from the fringe. Also it is clear that the revised magnet shape successfully eliminates the voltage ripple and restores the trapezoidal waveshape.

4.2.2 Assembly: Fitting the magnets in place was found to be a very difficult operation because of their mutual repulsion. An important consideration in all future designs will be to restrict the poles to a size which can be built in a single piece. To hold the poles during assembly, it was found necessary to mill shallow recesses on the face of each disc; this expensive operation will be unnecessary with single-piece magnets.

The magnets are glued in position. For high-speed or large-diameter designs, centrifugal shear stress in the glue would restrict the permissible thickness of magnet and it might still be necessary to mill recesses to provide additional mechanical support.

Consideration was given to assembly of the whole machine. The force of attraction between each rotor disc and the stator can be several kN even for machines of just 2.5 kW weighing less than 7 kg. Jacking screws must be provided to control the movement of components otherwise damage is almost certain.
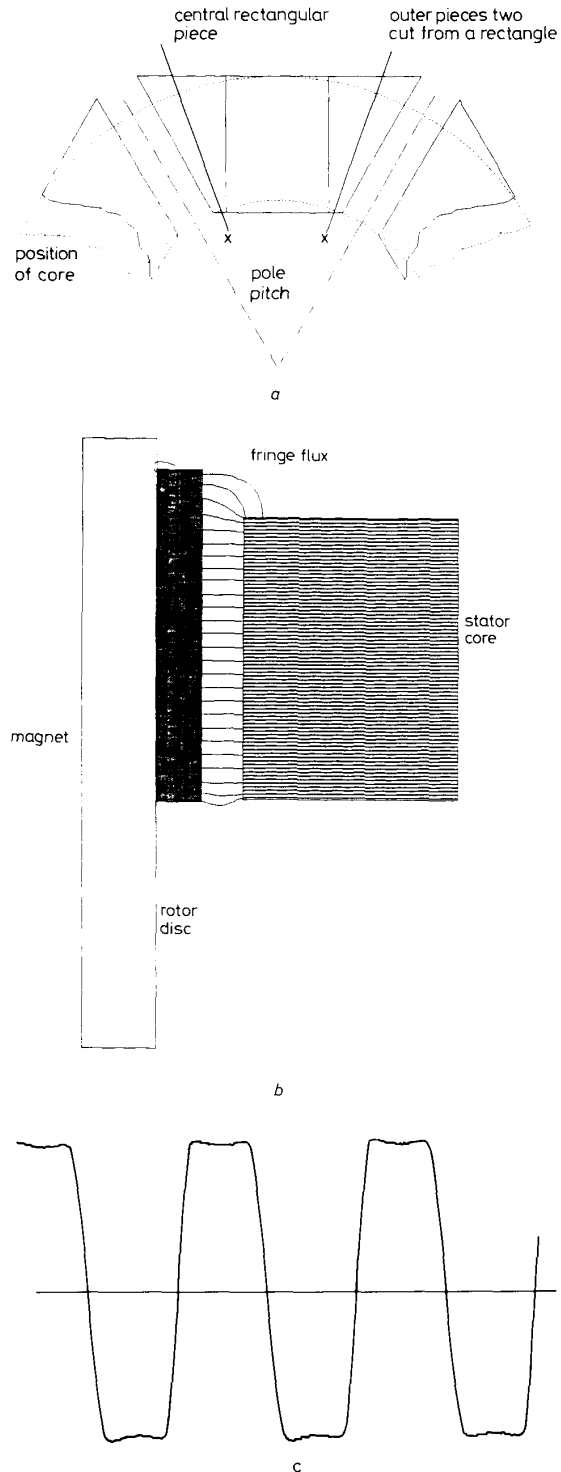
Fig. 5 *Magnet arrangement for Machines 1 and 2*

a Three-piece magnet shape
b Overhang producing fringe flux
c Induced EMF for one phase

4.3 Winding configuration

Each phase of the winding has two coils connected in series. The two coils are connected in opposition so that no flux tends to pass around the core when current flows. EMFs induced in the two coils add together to produce
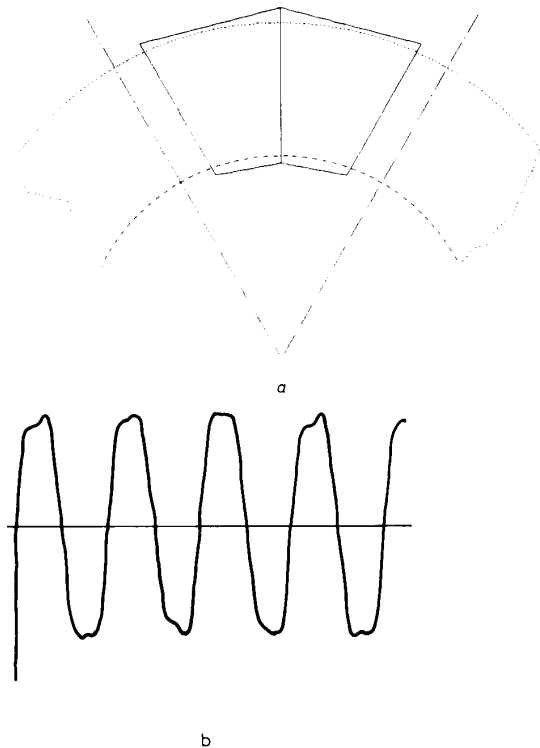

Fig. 6 *Magnet arrangement for Machine 3*

a Two-piece magnet shape
b Induced EMF for one phase

the phase terminal EMF if the rotor magnets passing the two coils are of opposite polarity. Since the coils are located diametrically opposite each other as shown in Fig. 7 only pole numbers of 2, 6, 10, 14 etc. satisfy this condition.
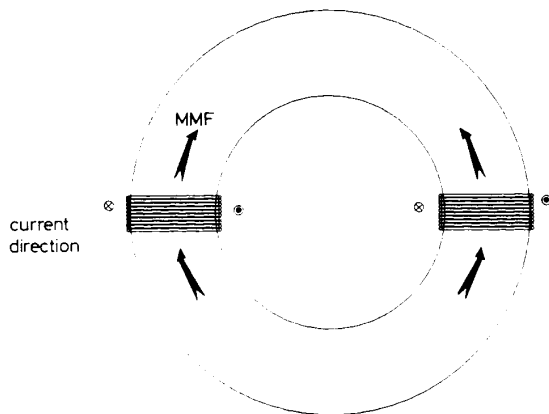

Fig. 7 *Stator winding arrangement for one phase*

5 Electrical performance

The theory of alternator performance with rectifier loading was established by Bonwick *et al.* [7, 8]. Kettleborough *et al.* [9] developed mathematical models for both transformers and for alternators feeding rectified

loads. These contributions were restricted to the case of three-phase, sinusoidal systems and their principal objective was to predict distortion of the AC voltage waveforms.

In developing the TORUS machine for generator applications, it has become clear that existing theories do not apply to this unusual non-sinusoidal, multiple-phase machine. Critical performance requirements are high efficiency, low output voltage regulation and low ripple content rather than low distortion of the AC waveform. The following simple analytical treatment ignoring phase-to-phase coupling was developed to estimate regulation, ripple and phase RMS current for use in assessing a range of design options.

5.1 Phase current

If the winding self and mutual inductances were ignored, then the DC terminal voltage could be obtained by considering the set of diodes connected to the positive line as acting as a large OR gate selecting the phase or phases with the greatest potential. However, the winding resistance and inductance can seriously distort the resulting simple rectangular current waveform. One simple condition can be dealt with analytically to illustrate how the phase inductance affects the performance. The output voltage is assumed to be pure DC, as could occur in practice if a large capacitor were connected to the terminals or if the machine were being used for battery charging. Also, we neglect the effects of mutual inductance and diode voltage drop. It is assumed that the windings are connected in star and that the star point is connected to the centre point of the load.

If the current in phase A, say, is considered to be initially zero, then, when the EMF first exceeds the output voltage, the current begins to rise at a rate determined by the difference between the induced EMF and the output voltage. The EMF is assumed to follow a simple trapezoidal waveform with plateau value E and plateau width a fraction, u, of the half cycle (corresponding to a duration T for frequency f). The output voltage is V, a little less than E. The current increases as

$$I = I_{dc}\{1 - \exp(-t/\tau)\} \tag{7}$$

where

$$I_{dc} = (E - V)/r \tag{8}$$

and

$$\tau = L/r \tag{9}$$

The current reaches a maximum value of

$$I_{pk} = I_{dc}\{1 - \exp(-T/\tau)\} \tag{10}$$

During this period the charge transferred, expressed as a mean current over a full cycle, is

$$I_{mean, 1} = f(I_{dc}T - I_{pk}\tau) \tag{11}$$

and the energy dissipated as I^2R loss is

$$Q_1 = r(I_{dc}^2 T - I_{dc}I_{pk}\tau - I_{pk}^2\tau/2) \tag{12}$$

At the end of the plateau period, the induced EMF falls linearly at a rate γ, V/s,

$$\gamma = 4fE/(1 - 2fT) \tag{13}$$

The EMF reaches zero after a time

$$t_E = E/\gamma \tag{14}$$

The current follows a complex curve

$$I = \{\gamma\tau/r + I_{dc} - \gamma t/r\}$$
$$\quad - \{\gamma\tau/r + I_{dc} - I_{pk}\} \exp{(-t/\tau)} \qquad (15)$$

to become zero after a time t_1. If, as in the experimental machines, the resistance is small than the time t_1 can be estimated from an approximate expression for current which ignores the resistance:

$$I = I_{pk} + \{(E - V)/L\}t - (\gamma/2L)t^2 \qquad (16)$$

If the time, t_1, rquired for the current to be brought to zero does not exceed the available time during which the EMF changes linearly to reach its plateau in the opposite direction, $2t_E$, then the current will reach and remain zero until the EMF becomes sufficient to cause the rectifier of opposite polarity to conduct and a new half cycle to begin.

Since the current varies approximately quadratically during this period, the mean current is 2/3 the peak, and the charge transferred, expressed as a mean current over the cycle, is

$$I_{mean,\,2} = f2I_{pk}/3t_1 \qquad (17)$$

The sum of $I_{mean,\,1}$ and $I_{mean,\,2}$ yields the mean current delivered by each phase to the positive terminal of the rectifier output. The total output DC current is the product of the number of phases and $(I_{mean,\,1} + I_{mean,\,2})$.

The energy dissipated during the period of falling current is approximately

$$Q_2 \doteq (8t_1/15)rI_{pk}^2 \qquad (18)$$

The RMS phase current may be found from Q_1 and Q_2

$$I_{rms} = \sqrt{\{2(Q_1 + Q_2)f/r\}} \qquad (19)$$

The output DC voltage is twice the voltage V since V represents the voltage between the positive terminal and the star point. To estimate the output voltage regulation we may use the above analysis with voltage as the independent variable, checking that the condition $t_1 < 2t_E$ is satisfied for each value. Also the phase RMS current may be found, using eqns. 12, 16, 18 and 19, and related to the output current.

5.1.1 Output voltage regulation: For the experimental machines the parameters given in Table 1 have been used to predict the regulation characteristics. It is found that the condition $t_1 < 2t_E$ holds throughout the range of interest and well beyond. A total diode voltage of 2 V is assumed. In each case the predicted output voltage varies almost linearly with load current. The predicted effective series resistance for each machine is given in Table 3 along with the slope of the measured characteristic and the percentage voltage regulation from no load to full-load current. The discrepancy by about a factor of two between predicted and measured effective resistance for Machine 3 is due to the mutual interaction between phases causing the waveform to be close to a 120° rectangular shape, rather than the approximately triangular shape of the analysis.

5.1.2 RMS phase current: The same parameters also yield the following ratios (Table 4) between output DC current and phase RMS current for full-load operation, although the ratio changes very little with load. From the measured values it can be seen that the prediction is close for Machines 2 and 3. The discrepancy for Machine 1 is due to the analysis not taking account of interactions

between phases which, in that case, lead to discontinuities in the phase current (see Fig. 4).

5.2 Current ripple

If the phases conduct for periods which do not overlap each other then the current reaching the DC side of the rectifier bridge will vary between zero and I_{pk}. The peak-

Table 3: Experimental machine effective series resistance (mΩ) and regulation

Machine	Predicted	Measured	Regulation, %
1	139	149	40
2	191	167	30
3	150	80	21

Table 4: Experimental machine RMS/DC current ratio

Machine	Predicted	Measured
1	0.227	0.276
2	0.257	0.266
3	0.262	0.265

to-peak amplitude of the current ripple in this case is simply I_{pk}.

If there are m phases, then the electrical angle between successive phases is $360°/m$, which at frequency, f, corresponds to a time of $1/mf$ second. For Machine 1 with 11 phases the angle is 33° but the angle of the plateau is 112° so there will be three or four phases conducting current to the positive DC line at any instant and three or four conducting to the negative line.

The total current flow is found from the sum of the separate phase currents separated in time by $t_p(-1/mf)$. For the period when four phases carry currents on the rising section of the wave, eqn. 8 may be used to give the individual phase currents and their sum is:

$$I = I_{dc}\{1 - \exp{(-t/\tau)}\} + I_{dc}\{1 - \exp{[-(t - t_p)/\tau]}\}$$
$$\quad + I_{dc}\{1 - \exp{[-(t - t_{2p})/\tau]}\}$$
$$\quad + I_{dc}\{1 - \exp{[-(t - t_{3p})/\tau]}\} \qquad (20)$$

The maximum current occurs just as the most advanced phase reaches peak current and is about to cease conducting. Using that phase for time reference, maximum occurs at $t = T$. Minimum current occurs immediately after the switch off and so, if switch off is very rapid, the minimum occurs also at $t = T(+)$. The total current therefore forms a sawtooth wave with amplitude

$$I_{rip} = I_{dc}\{1 - \exp{(-T/\tau)}\} \qquad (21)$$

This is identical to eqn. 10, so that the DC output ripple current I_{rip} has a peak-to-peak value equal to the peak current of a single phase. Expressed as a fraction of the mean DC current, therefore, the ripple current is inversely proportional to the number of phases.

5.3 Output voltage ripple

If the machine no longer feeds a constant-voltage load, then ripple voltage may appear at the terminals. Its magnitude will depend on the ripple current and the impedances of the load and the machine to the ripple current. An estimate of the ripple voltage can be obtained by respresenting the machine as a source of ripple voltage in series with an impedance; i.e. as a Thevenin source. The

preceding analysis, where the output voltage is assumed constant, gives the short-circuit ripple current of the source.

The frequency of the ripple voltage, f, as measured between either DC line and the winding star point, is equal to the number of phases times the frequency of the phase current and the ripple waveform is assumed to be sinusoidal for simplicity. The series impedance consists of the parallel combination of the impedances of all the phases which are conducting. Thus, for Machine 1 with three or four phases conducting, the impedance is between one third and one fourth of $(90 + j2\pi f 120 \times 10^3)$ mΩ. The resulting values of ripple voltage between the star point and one of the DC output terminals are given in Table 5 for the case of a pure

Table 5: Experimental machine Pk-Pk ripple voltage

Machine	Current (A)	Calculated	Measured
1	0	0.0	0.9
1	15	6.2	1.5
2	20	3.1	3.0
2	55	7.7	4.0

resistive load at several current values for each of the experimental machines.

However, the ripple voltage for resistive load departs markedly from a sinewave and most of the discrepancy can be attributed to harmonics of the basic ripple frequency. In some applications the ripple may be filtered by means of a capacitor connected across the terminals. This suppresses the harmonics as may be seen by comparing the ripple waveforms given in Fig. 8a and b. The analysis produces much closer results in this case as shown in Table 6. The subharmonic ripple seen in Fig. 8

Table 6: Experimental machine Pk-Pk ripple voltage with terminal capacitors connected

| Machine	Current (A)	Capacitance (mF)	Calculated	Measured
1	20	4.4	0.59	0.3
1	55	4.4	1.93	0.6
1	20	8	0.27	0.2
1	55	8	0.65	0.4

is attributed to the lack of precise equality of the magnet poles.

5.4 Efficiency

For the precise measurement of efficiency of the experimental machines, the arrangement shown in Fig. 9 was used. The cooling fans of the totally enclosed, fan-cooled drive motors were removed for coupling and a torque transducer inserted in the drive chain. For measurements on machine A, for example, the drive motor of machine B would be energised. The windage and friction loss of drive motor A is included in the torque measured and is subtracted later. The torque associated with windage and friction in each drive motor was found by separate tests for which the experimental generators were removed. The total no-load loss, eddy current, iron and windage was then obtained after replacing the experimental machine.

Machines 1 and 3 have been used for measurements of losses and efficiencies. Results for no-load loss and efficiencies at several values of load current are given in

Table 7 and compared with predicted values. The measurements were taken after temperatures had stabilised to the values given in Section 6. The predicted efficiencies are based on the measured output power and the predicted no-load losses in Section 3.5 adjusted for a winding temperature of 100°C.
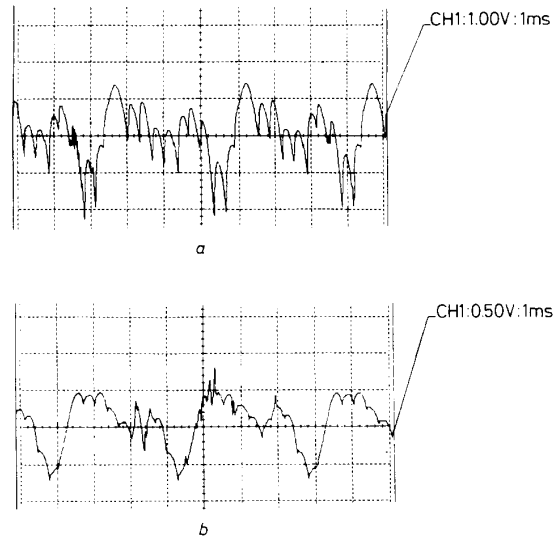
Fig. 8 Output voltage ripple
a Machine 2, 20 Amp load, no capacitor
b Machine 2, 20 Amp load, 4.4 mF capacitor
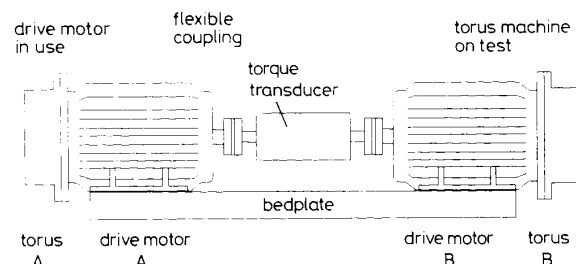
Fig. 9 Loss and efficiency test arrangement

Table 7: Experimental machine efficiencies

Machine	1	3
Measured no-load loss, W	85	93
Predicted no-load loss, W	67	88
Efficiencies %		
measured efficiency	74.0	77.5
test current, A	45.0	45.0
predicted efficiency for test current	81.3	83.8
measured efficiency	73.5	78.3
test current, A	62.0	63.3
predicted efficiency for test current	78.7	83.1
measured efficiency	68.7	74.5
test current, A	88.7	93.3
predicted efficiency for test current	72.8	80.2

The efficiency discrepancies for Machine 1 all correspond to a torque error of 0.5 Nm, whereas those for Machine 3 correspond to torque errors between 0.4 and 0.7 Nm. Alternatively, the errors may all be expressed as discrepancies in total loss of between 120 and 200 W. In view of the declared accuracy of the torque sensor of 1% of its 20 Nm full scale and the unavoidable small errors

in the other measurements involved, the results are considered a satisfactory validation of the loss and efficiency predictions.

6 Thermal performance

6.1 Ventilation
An air stream is needed for removal of losses and heat conducted through the casing or shaft from the engine. The rotation of the two magnet discs naturally acts as a fan, the magnets behaving as impeller blades. The path of the air stream is indicated in Fig. 10. The pressure head
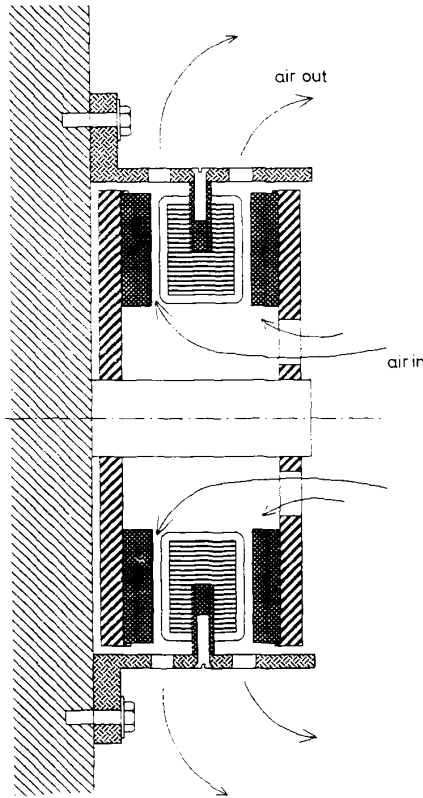

Fig. 10   *Ventilation paths*

created by the discs rotating at the nominal speed is found, using the method outlined by Grayer [10], for Machines 1 and 2 to be approximately

$$P = 270 - 13\,600F - 308\,000F^2 \qquad (22a)$$

For Machine 3, which is rather smaller in diameter,

$$P = 220 - 11\,200F - 250\,000F^2 \qquad (22b)$$

The resistance to airflow comprises pressure drops at the following positions
   (a) Air inlet holes on one disc
   (b) Changing direction on entry into stator-rotor gap space
   (c) Expansion leaving airgap space
   (d) Exit through holes in casing

The pressure drop through the machine is given in Reference 10

$$P = \Sigma(K/A)^2 F^2 \qquad (23)$$

where K is a factor for each of the above sections of the air flow path depending on the geometry. For all three machines the sum is estimated using expressions derived from Reference 10 to be approximately 2.4×10^6 (N/m^2)/ (m^3/sec)^2. In each case it is the entry into the gap space which dominates.

The airflow is found from the above fan and resistance characteristics to be about 0.0087 m^3/sec for Machines 1 and 2 and about 0.0079 m^3/sec for Machine 3. Both figures are subject to some uncertainty. With the above rate of flow in Machines 1 and 2, the air will rise in temperature by roughly 0.095°C for each Watt of heat which is absorbed. For Machine 3 the figure is 0.11°C. If all the heat generated were to be absorbed by the air then we should expect exhaust temperatures to exceed inlet temperatures by 69°, 50° and 54° for Machines 1, 2 and 3 respectively.

6.2 Thermal model
The copper and iron losses are removed principally by forced convection at the two airgap surfaces of the stator. Some is transferred to the air at the inner cylindrical surface and some passes by conduction to the casing to be removed by the cooling air along with the rectifier losses and heat flowing from the engine.

Fig. 11 shows the lumped-parameter network of thermal resistances used for the predetermination of
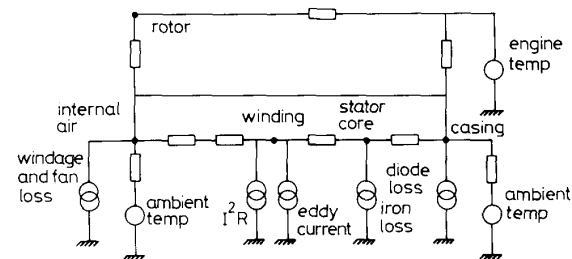

Fig. 11   *Lumped-parameter thermal model*

steady-state operating temperatures. Resistances associated with conduction through solids are calculated from the dimensions and thermal conductivity of the material. All insulating materials are assumed to have a thermal conductivity of 0.2 W/mK, and metals are assumed to have infinite conductivity. Resistances which represent the transfer of heat from a solid surface to the cooling air are calculated using a value of 150 W/m^{2}K for the heat transfer coefficient. Resistances between adjacent solid bodies such as where the metal dowels make contact with the stator laminations are also evaluated using a heat transfer coefficient of 2000 W/m^{2}K. These figures were arrived at after a series of tests carried out using an instrumented dummy machine. A notional resistance is used to represent the path for heat flow between the engine casing and the generator casing and a further notional resistance is used to represent the path along the shaft from the engine crankshaft.

A resistance is shown to represent the increase in air temperature as it absorbs heat passing through the machine. However, the model used for design and performance calculations simply employs a figure for internal air temperature rather higher than ambient. This is done because a substantial heat flow into the air takes place close to the exhaust point and it would be unreasonable to allow this to reflect upon the average air temperature within the machine.

Table 8: Predicted temperatures for the experimental machines

Machine	Current	Winding	Casing
1	89.3	132	88
2	71.4	113	79
3	89.3	136	91

The model predicts the temperatures given in Table 8 for the three machines working at their nominal full-load currents; in each case the engine is assumed to be at a temperature of 75°C. The ambient temperature is taken to be 30°C and the air inside the machine is taken to be at 40°C.

6.3 Temperature rise tests

Each machine has been operated continuously to determine winding temperature over a range of current. It takes about one hour to reach thermal equilibrium. Temperatures are measured by resistance periodically during each run. The test conditions cannot accurately model the complete working situation of the machine because the drive motor casing does not reach temperatures typical of a combustion engine. However, the model is found to be not particularly sensitive to engine temperature.

Test results for winding temperature rise above ambient are compared with corresponding model predictions below. It can be seen that the model gives adequate accuracy for most purposes and errs on the side of caution. The measurements are systematically less than predicted, one possible cause being the fall in temperature during the short period between shutdown and taking the measurement. No corrections for this have been applied to the measurements at this stage.

Table 9: Experimental machine winding temperatures

Test	Machine	Current A	Temperature rise, °C, above ambient	
			Predicted	Measured
1	1	52	57	44
2	1	70	80	78
3	2	44	36	44
4	2	56	60	50
5	2	72	86	62
6	2	80	101	95
7	3	45	46	36
8	3	76	87	62
9	3	89	115	98

7 Conclusion

The combination of the new high-field permanent magnet material with the slotless winding makes for a very compact machine. The toroidal machine naturally generates a high-volume flow of cooling air through the active parts. The simple lumped-parameter thermal resistance network predicts winding temperature rise with adequate accuracy for design purposes and with errors which leave a margin for safety.

8 References

1 CAMPBELL, P.: 'Principles of a permanent-magnet, axial-field dc machine', Proc. IEE, 1974, 121, (12), pp. 1489–1494
2 EVANS, P.D., and EASTHAM, J.F.: 'Slotless-disc alternator with AC-side excitation', IEE Proc. B, Electr. Power Appl., 1983, 130, (6), pp. 399–406
3 SPOONER, E., and CHALMERS, B.J.: 'Toroidally-wound, slotless, axial-flux, permanent-magnet, brushless-dc motors'. Proc. Int. Conf. Elec. Machines, Pisa Sept 1988, Vol. II, p. 81
4 SPOONER, E., and CHALMERS, B.J.: '"TORUS", a toroidal-stator, permanent-magnet machine for small-scale power generation'. Proc. Int. Conf. Elec. Machines, MIT, Cambridge, USA, Aug. 1990. Vol III, p. 1053
5 LAITHWAITE, E.R.: 'Induction machines for special purposes' (Newnes, 1966), p. 38
6 SPOONER, E.: 'The dc traction motor with slotless armature', IEE Proc. B, Electr. Power Appl., 1985, 132 (2), pp. 61–71
7 BONWICK, W.J., and JONES, V.H.: 'Performance of a synchronous generator with bridge rectifier', Proc. IEE, 1972, 119, (9), pp. 1338–1342
8 BONWICK, W.J.: 'Characteristics of a diode-bridge-loaded generator without damper windings', Proc. IEE, 1975, 122, (6), pp. 637–642
9 KETTLEBOROUGH, J.G., SMITH, I.R., and FANTHOME, B.A.: 'Simulation of a aircraft generator supplying a heavy rectified load', IEE Proc. Electr. Power Appl., 1983, 130, (6), pp. 431–435
10 GREYER, I.W.: 'Materials and motor components', in CHALMERS, B.J. (Ed.): 'Electric motor handbook' (Butterworth, 1988), pp. 310–311
11 CLAYTON, A.E.: 'Performance and design of direct current machines' (Pitman, 1959, 3rd edn.), p. 244

Appendix: torque calculation

Consider a radial element, δr, of one face of the stator and an angular element $\delta\theta$. The force exerted between the rotor and the elementary area of the stator is found using

$$F = Bil$$

where $B = B(\theta)$, $i = r\delta\theta J_s(r, \theta)$ and $l = \delta r$.

Hence the torque due to the force on that element is

$$\delta T = B(\theta)J_s(r, \theta)r^2\delta r\delta\theta$$

The winding conductors pass radially across the face of the stator and so the electric loading at radius r is inversely proportional to r. The wires are placed as close together as possible at the bore of the stator and so it is the electric loading, J_1 at the inner radius, R_1 which is the important design parameter. The torque can therefore be written:

$$\delta T = B(\theta)J_1(\theta)rR_1\delta r\delta\theta$$

$$= B(\theta)J_1(\theta)\delta\theta R_1 r\delta r$$

Integrating over the full radial extent of the stator face:

$$\delta T = B(\theta)J_1(\theta)\delta\theta\tfrac{1}{2}R_1(R_2^2 - R_1^2)$$

Both $B(\theta)$ and $J_1(\theta)$ are distributed periodically. The integral of their product around the stator will depend upon the details of the distributions. If the flux density is trapezoidal in distribution with maximum value B, and the current is concentrated into regions where the flux density is at the maximum value then the integral simplifies to

$$B_{max}J_1 2\pi$$

where J_1 is the average electric loading over a pole pitch at the stator bore.

The total torque generated by the two faces of the stator in this case is therefore

$$T = BJ_1 2\pi R_1(R_2^2 - R_1^2)$$